Controlled Growth of Single-Crystal Twelve-Pointed Graphene Grains on a Liquid Cu Surface

Dechao Geng, Lan Meng, Bingyan Chen, Enlai Gao, Wei Yan, Hui Yan, Birong Luo, Jie Xu, Huaping Wang, Zupan Mao, Zhiping Xu, Lin He, Zhiyong Zhang, Lianmao Peng, and Gui Yu*

Graphene, a perfect two-dimensional atomic crystal, has attracted considerable attention due to its unusual mechanical, optical, and electronic properties.[1] To synthesize high-quality graphene, mechanical exfoliation of highly oriented pyrolytic graphite,[1] chemical reduction of graphene oxide,[2,3] and chemical vapor deposition (CVD)[4,5] have been developed. Among those approaches, the CVD method possesses great potential in graphene growth and application because of the low-cost and high-scalability. However, the graphene thin film prepared by the CVD method using metal catalysts is composed of numerous grain boundaries, which largely compromise performance of graphene-based electronics as structure defects. Therefore, to enhance electronic properties of graphene-based devices, investigations on growth of single-crystal graphene grains have been motivated. Recent advances in the CVD method have enabled the preparation of single-crystal graphene grains with several shapes.[6–18] Among those grains, hexagonal graphene has been the most extensively explored since it was observed on solid copper (Cu) foil.[6–10] Apart from that, triangular,[11,12] rectangular,[13–15] four-lobed,[16] and snow-like graphene grains[17,18] have been achieved, demonstrating the great potential in shaping graphene using CVD approach on metal substrates.

As precise control of graphene shape is the key capability of investigating the growth mechanism,[19] fabricating single-crystal graphene grains with new shapes have received intensive efforts. However, it remains extraordinarily challenging to precisely control the process details in the graphene growth, which could largely affect the characteristics of as-grown graphene. On the other hand, although recently the mechanism of shape change for graphene grains has been reported,[20,21] the relationship among those shapes needs to be further evidenced. Here the twelve-pointed graphene grains (TPGGs) were first controllably synthesized using ambient pressure chemical vapor deposition and the growth mechanism was proposed. Liquid Cu was employed as a catalyst to prepare graphene.[22,23] The growth temperature was kept at 1120 °C, at which the solid Cu foils were changed into liquid phase. The growth of TPGGs was initiated by introducing 3–5 sccm CH_4 gas flow into the chamber with the H_2 flow rate held at 300 sccm for 3–5 min.

The images of as-grown TPGGs are clearly shown in **Figure 1**. The scanning electron microscopy (SEM) images (Figure 1a) indicate that the TPGGs are well-dispersed on the whole Cu surface. Most of the graphene grains have the similar edge-to-edge distances, suggesting homogeneous nucleation. The appearance of the TPGGs demonstrates the high versatility of graphene growth by the CVD method and enlarges the shape family of graphene grains. Further, the growth of large-scale TPGGs displays the high controllability over graphene shape using the liquid metal catalysts under certain CVD growth conditions (Table S1). For the as-grown graphene grains, size statistics (Figure S1a) shows that the average size falls into the range from 30 to 40 μm, which is largely determined by carbon source flow rate and the growth time. Related model of graphene growth has been established to explain the growth process on Cu surface based on important growth factors.[7,8] It is suggested that graphene nucleation density and growth rate are finally responsible for the graphene grain size. According to the model, growth conditions are still optimized for growth of larger size TPGGs. It is believed that the millimeter-scale grains could be available through narrowing the carbon source window and increasing growth time.

As shown in Figure 1b, the single TPGG shows extremely high twelve-folded symmetry, demonstrating an unrevealed graphene growth rule under the certain growth conditions. For single TPGG, the six diagonal distances (Figure S1b) are identified as AG, BH, CI, DJ, EK and FL, respectively. The diagonal distances of 15 graphene grains were calculated and the data are listed in Table S2. We can see that the standard deviation is rather low for each single TPGG, further demonstrating the high symmetry. We first used optical spectroscopy to measure the uniformity and layer numbers of these TPGGs.

D. C. Geng, B. R. Luo, J. Xu, H. P. Wang,
Z. P. Mao, Prof. G. Yu
Beijing National Laboratory for Molecular Sciences
Institute of Chemistry
Chinese Academy of Sciences
Beijing 100190, P. R. China
E-mail: yugui@iccas.ac.cn
L. Meng, W. Yan, H. Yan, Prof. L. He
Department of Physics
Beijing Normal University
Beijing 100875, P. R. China
B. Y. Chen, Prof. Z. Y. Zhang, Prof. L. M. Peng
Key Laboratory for the Physics and Chemistry of Nanodevices
Department of Electronics
Peking University
Beijing 100871, P. R. China
E. L. Gao, Prof. Z. P. Xu
Applied Mechanics Laboratory
Department of Engineering Mechanics and Center
for Nano and Micro Mechanics
Tsinghua University
Beijing 100084, P. R. China
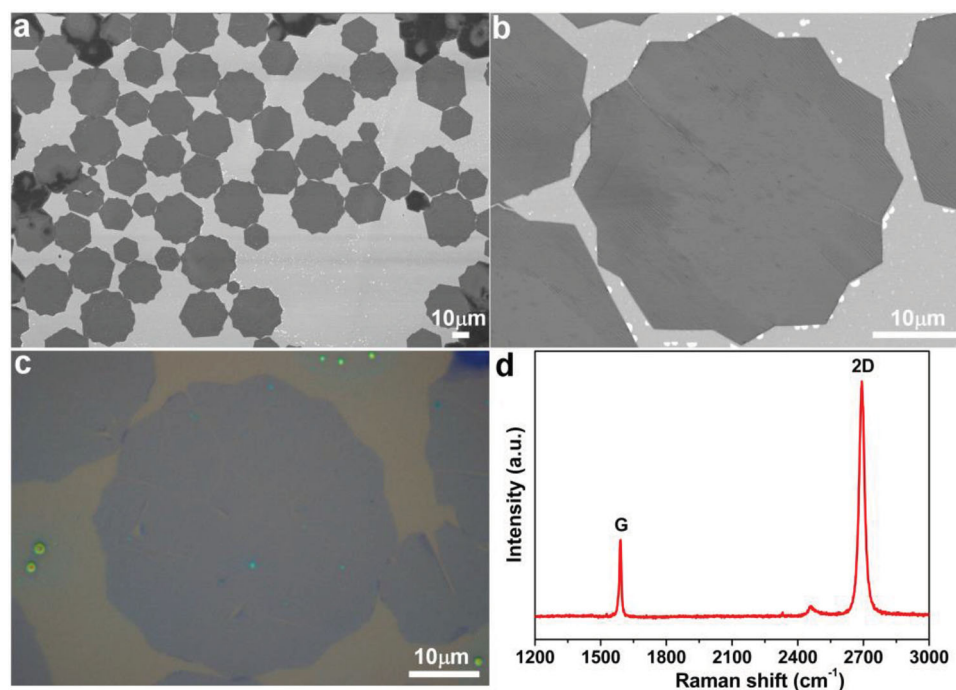
Figure 1. Twelve-pointed graphene grains. (a and b) SEM images of as-grown TPGGs on the Cu surface. (c) Optical image of the TPGG transferred onto 300 nm SiO_2/Si substrates. (d) Raman spectrum of single TPGG.

The TPGGs were transferred onto SiO_2/Si substrate by using electric-chemical bubbling method.[24,25] Figure 1c shows the optical microscope image of single TPGG. The contrast of the image is uniform and there exists no color variation across the whole single TPGG, indicating single-layer characteristics. To further identify the layer number, Raman spectrum measurements were conducted. In our experiments, Raman measurements using a 514 nm excitation laser were performed on transferred TPGGs. The Raman spectrum is clearly shown in Figure 1d. The TPGG displays typical single-layer features with two prominent Raman peaks located at 1580 and 2680 cm^{-1}, corresponding to the G and 2D peaks, respectively. The intensity ratio of I_{2D} and I_G is about 3–5 and no D peak related to its defect was detected, indicating single-layer and high-quality features of as-grown TPGGs. Atomic force microscopy (AFM) is a non-destructive technique to probe the surface morphology in nanoscale. Clear contrast between the TPGGs and substrate surface was observed (Figure S2a,b), suggesting the uniform surface among the whole TPGG. Height profiles across patterned graphene edges was performed as shown in the Figure S2c, in which the thickness of the TPGG sample is about 0.587 nm, which is consistent with the monolayer range.[7]

To further characterize these TPGGs, we used a combination of transmission electron microscopy (TEM), Raman mapping, and scanning tunneling microscopy (STM) as shown in **Figure 2**. Prior to TEM observations, transferred TPGG samples were located by SEM, as shown in Figure 2a. The brighter contrast of graphene on holey supporting films exhibits twelve-pointed shape, indicating the successful transfer of graphene. The exact position of single TPGG on the TEM grid can be determined from the SEM images, which facilitates TEM characterizations because graphene is difficult to identify in a

normal bright-field TEM view field. Then selected-area electron diffraction (SAED) patterns show the same six-fold symmetric diffraction points at different regions marked **1–3** over the entire TPGG (Figure 2b-d). The results demonstrate that the TPGG contains no rotational boundaries to within our measurement accuracy of 0.5°. We have also tested many individual TPGGs and found that all of them show the single-crystalline feature from the SAED results. Raman mapping was also conducted on the transferred TPGGs (Figure 2e) for more information, in which the intensity mapping of the three characterized peaks of D, G, and 2D are clearly shown in Figure 2f-h. The G and 2D peak mapping show the high uniformity across the whole TPGG while the inconsistence in D peak mapping due to the residues left during the transferring process. The typical intensity ratio (I_{2D}/I_G) within a TPGG is larger than 2, indicating that our samples are single-layer graphene. Further, STM was employed as an effective method to characterize the as-grown TPGGs on the Cu surface. Observation of the large-scale morphology of the TPGG samples was accomplished over hundreds of square nanometers (Figure 2i). Then the perfect carbon honeycomb lattice was clearly found from the atomic-resolution images of different regions (Figure 2j-l). In both low and high magnification STM images, we didn't observe any defects or boundaries in the plane, suggesting the monolayer and single-crystalline features of the TPGGs. It should be noted that the blunt TPGGs were also observed as shown in Figure S3. Comparing to the typical TPGGs, the appearance of those blunt grains could be related with the local dominance of hydrogen-etching over graphene growth.[8,26–28] As pointed out in a recent work,[21] the emerging edge during this process is the fast-etching one with ~19° slanted angle measured from zigzag edges. The shape of TPGG is then smoothed. Both
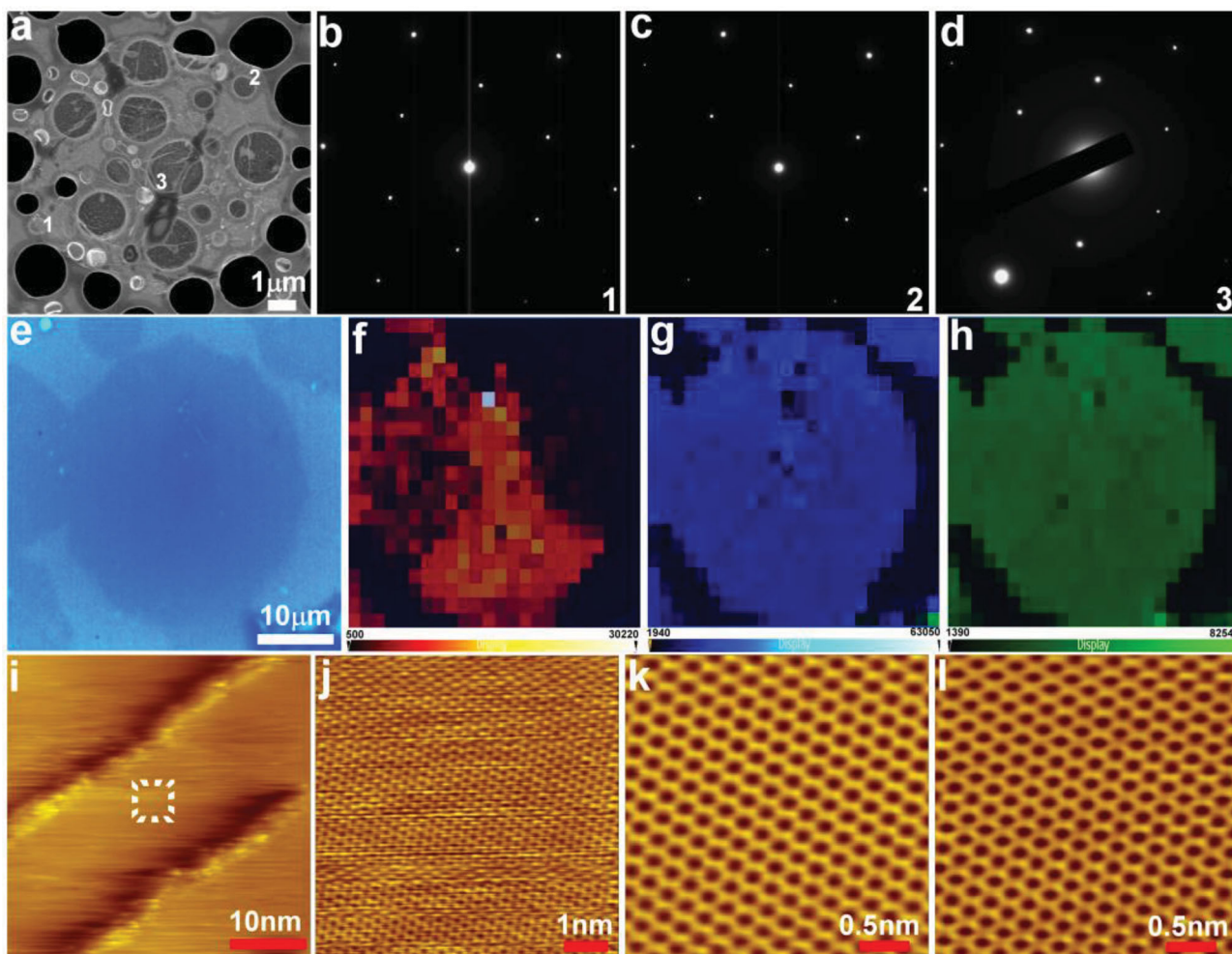
Figure 2. SEM, TEM, Raman mapping, and STM images of the TPGGs. (a) SEM image of the TPGGs on a copper TEM grid. (b-d) SEAD data for small regions of single TPGG indicated 1 to 3. (e) Optical image of the TPGG transferred onto 300 nm SiO$_2$/Si substrates. (f-h) Intensity mapping of the D, G and 2D Raman peaks, respectively, for a single crystal grain. (i-l) Atomic-resolution STM images of the TPGGs on the Cu surface. STM imaing parameters: (i) I_t = 17 pA, V_s = 900 mV; (j-l) I_t = 17 pA, V_s = − 650 mV.

armchair and zigzag edges could evolve into the fast-etching edge-type. To suppress this blunting process and maintain the sharp alternative armchair-zigzag edges, the amount of hydrogen should be kept at a lower level over the whole growth region. Electron diffraction data (Figure S4) further show the single-crystalline features of those blunt grains.

Our previous experiments suggested that the hexagonal graphene grains could be precisely fabricated on liquid Cu.[22] In this work, the TPGGs can be also controllably prepared. The relationship between the hexagonal and TPGG was probed. The five kind shapes from hexagonal to twelve-pointed graphene were observed (**Figure 3**a–e). When carbon source flow rate gradually increases, an inter-edge of hexagonal graphene grain further grows to obtain a seven-pointed shape while simultaneous growth at two or more inter-edges could lead to formation of eight-, nine-, ten-, eleven-, or twelve-pointed graphene grains (Figure 3f). The growth mechanism will be detailed in the following section. Under optimized growth conditions, the methane flow rate was kept at 1 sccm, hydrogen flow rate at 300 sccm for 20–30 min, the hexagonal graphene grains were

successfully prepared as shown in Figure 3g. While increasing the carbon source flow rate to 3–5 sccm, the TPGGs gradually appeared (Figure 3h). When we further increased the methane flow rate to 6 sccm, the round shape graphene grains were clearly found over the Cu surface as shown in Figure 3i. The large-scale SEM images of the three kind as-grown graphene grains (hexagonal, twelve-pointed, and round) on the Cu surface are shown in Figure S5a-c, while the optical images of the corresponding transferred samples are also displayed (Figure S6). It is concluded that the carbon source flow rate is crucial for the shape change and grains size (Figure S5d). Recently, the evolution of graphene shape from hexagonal to round has been reported in which the middle stage was blunt hexagonal[17] or octagonal.[29] The appearance of TPGGs demonstrates a new path for graphene shape change on metal substrates by CVD method.

In order to understand the formation mechanism of TPGGs, we propose here an edge-diffusion limited model that explains the formation of tips and the critical grain size required.[30] After a grain nucleates with size beyond that of the
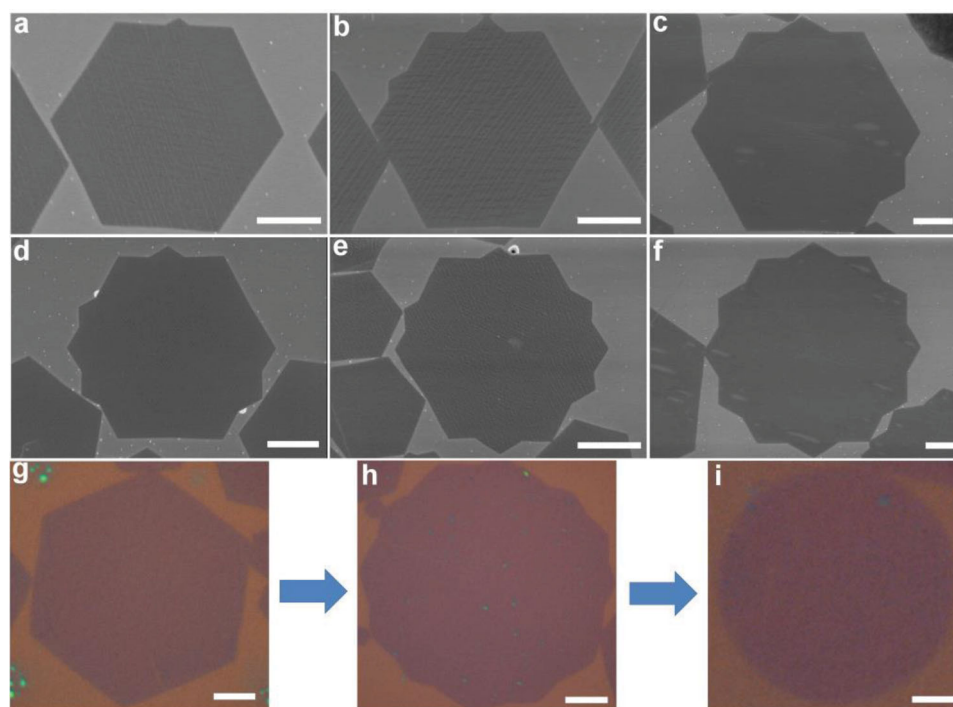
Figure 3. Formation of tips in hexagonal graphene grains. (a-e) Five types of graphene grains with different numbers of tips grown from hexagonal ones. (f) A twelve-pointed graphene grain. (g-i) Transforming process from hexagonal to round shaped graphene grain. All scale-bars are 5 μm.

critical nucleus, hexagonal grains continue to grow with zigzag edges.[21,31] The carbon atoms dissociating from carbon sources diffuse to the edge. Following the edge attachment, these newly arrived carbon atoms continue diffusing on the edge to reach the kink site. This last process is essential for the hexagonal grain to maintain its compact and facetted shape. Insufficient edge diffusion or kink sites would lead to morphological instability during the growth.[32,33] The total flux F of carbon atoms impinging onto the graphene edge with length L (including both the process of carbon deposition onto the substrate and its diffusion toward graphene edges) increases with carbon source flow rate in the experimental conditions. Considering a single graphene island in growth, the time scale between subsequent arrivals of the carbon atoms is $\tau_a = 1/F$. As the deposition rate per edge length f_e can be assumed as a constant during the growth, we have $F = f_e L$ and $\tau_a = (f_e L)^{-1}$. For the hexagonal grain to maintain its hexagonal shape, it should be assured for the adatom to find a kink site along the edge before the next atom arrives. The time scale for carbon atoms to diffuse over the edge with length L is $\tau_e = L^2/2D_e$. Here $D_e = \nu_0 \exp(-E_b/k_B T)$ is the one-dimensional diffusion constant along graphene edges, $\nu_0 = 5 \times 10^{12}$ s^{-1} is the attempting frequency, and E_b is the energy barrier for edge diffusion. Our density functional theory based calculations gives $E_b = 0.56$ eV and 2.02 eV for zigzag and armchair edges of graphene, respectively (see Supporting Information for details). These relatively high barriers compared to that of the thermal fluctuation (0.12 eV) for the growth temperature 1400 K indicate that the edge diffusion could be a rate-limiting process for the lattice perfection. Thus by comparing τ_a and τ_e, one would expect that when the edge length of a hexagonal grain exceeds a critical value $L_c = (2D_e/f_e)^{1/3}$, the local

triangular clusters or tips would nucleate (**Figure 4**a) and the edges of these tips are then fast-growing armchair ones (blue line indicated in Figure 4a and Figure S7). The unique edge characteristics of TPGG will lead to the effective property-engineering of graphene. Although quantitative prediction of the critical edge length is not feasible due to the lack of information about F or f_e, we can estimate $L_c = 12.5$ μm from SEM images taken for samples measured in experiments (Figure 4b). It is indicated from correlation between the tip numbers of grains and their edge lengths that, beyond L_c most of the grains own six tips, i.e. one tip for each edge. The exceptions with fewer tips are explained by the neighboring effect, where the value of F for specific edges is reduced because of the spatial confinement between neighboring grains.

This edge-diffusion limited mechanism for graphene grain growth can also be discussed with respect to experimental conditions. The formation of tips on the edges of hexagonal graphene with a specific edge length L is more preferred as the carbon flow rate or f_e increases as τ_a decreases compared to τ_e, which is consistent with the observations in Figure 3g, h. At a much higher carbon flow rate, sufficient carbon supply could take over the rate-limiting role and the grain growth becomes isotropic, yielding round-shaped grains (Figure 3i). In this regime, although increase of carbon flow rate accelerates the growth, stable grain growth requires a relatively low rate to avoid shape instabilities and formation of fractal-dendritic grains. This is why we keep a relatively low rate in the experimental conditions of this work.

In our experiments, the TPGGs were highly reproduced under the growth conditions, in which the monolayer grains made up nearly 95 percent. It should be noted that the bilayer

Materials
Views
www.MaterialsViews.com

ADVANCED
MATERIALS
www.advmat.de

COMMUNICATION
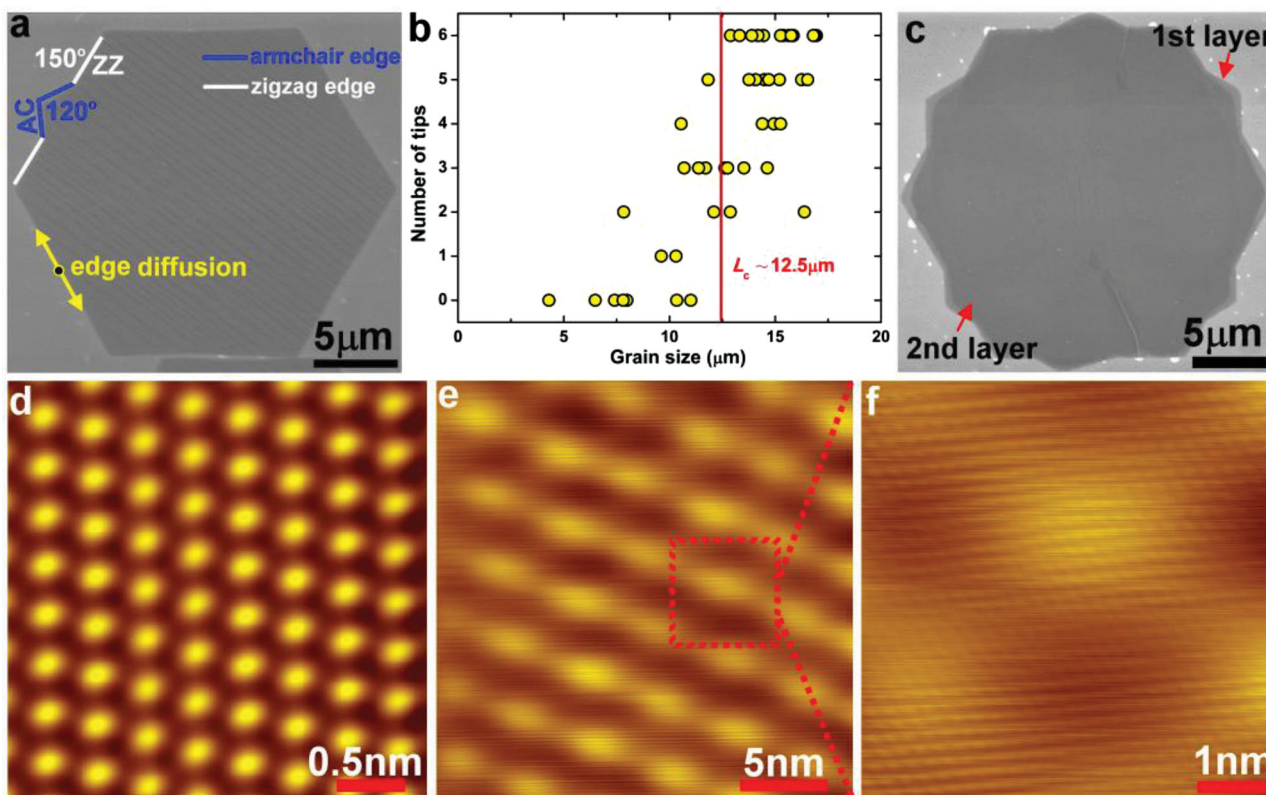
Figure 4. (a) Illustration of the edge-diffusion limited growth mechanism of TPGG. (b) Experimetal statistics between the number of tips appearing on the zigzag edges of the hexagonal grain, which shows a critical length scale L_c ~12.5 μm for edge diffusion of carbon atoms. It should be noted that when two grains meet during growth, the spatial constriction at the gap limits nucleation of the triangular islands and thus reduces the number of tips formed. (c) SEM image of the bilayer TPGG. (d) STM images of as-grown bilayer TPGGs. (e, f) Typical topographies of the bilayer TPGG showing a moiré pattern. STM imaging parameters: (d) I_t = 6.56 pA, V_s = 345 mV. (e) I_t = 9.73 pA, V_s = −458 mV. (f) I_t = 10.2 pA, V_s = −458 mV.

TPGGs were also found on the Cu surface as shown in Figure 4c. From the SEM and optical images (Figure S8a, b), the two layers could be clearly distinguished from the contrast difference. Raman spectrum on the transferred grain (Figure S8c, d) further verified the bilayer features. The atomic resolution STM image is shown in Figure 4d, in which the triangular lattices are detected rather than hexagonal, indicating that the bilayer graphene displays AB stacked mode.[34] Apart from that, clear moiré pattern with a period of 4.51 nm were observed as shown in Figure 4d, e. The period patterns are attributed to stacking mis-orientation between two graphene layers, confirming the bilayer characteristics.
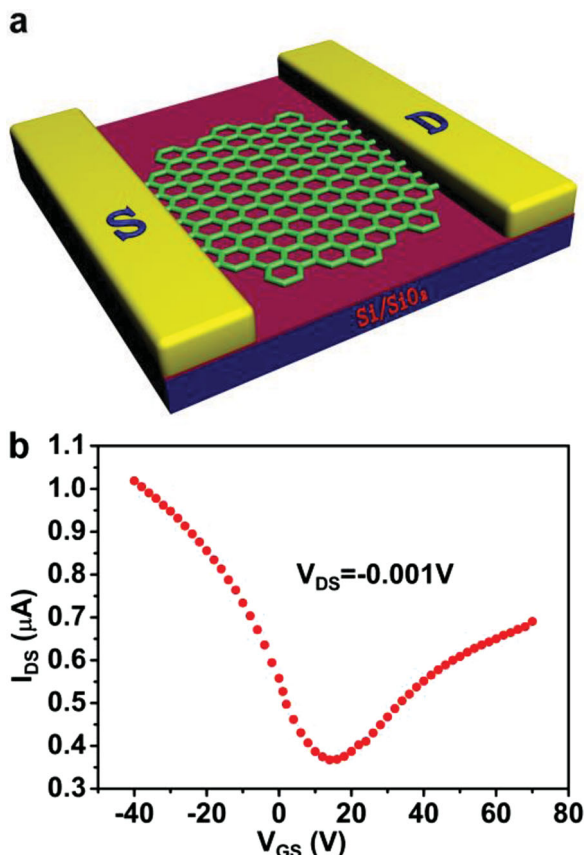
Electrical characterization was performed to probe carrier transporting feature on the individual graphene grain and thus field-effect transistors (FETs) were constructed as displayed in **Figure 5**. The FET structure is schematically illustrated in Figure 5a. The source and drain electrodes (Ti/Au, 5 nm/45 nm) were fabricated on the individual TPGG using conventional electron beam lithography. The devices were annealed in a vacuum to remove the absorbed molecules and field-effect performance was measured under N_2 at room temperature. Owing to p-type doping of the grain by the Ti/Au contact,[35] the device based on the transferred individual TPGG (Figure 5b) shows a Dirac point at a positive gate voltage (typically 10–20 V). The mobilities of the as-constructed FET devices are mainly

ranging from 2000 to 5000 cm^2 V^{-1} s^{-1} (Figure S9), which are comparative with those of single-crystal hexagonal graphene (Figure S10) recently reported.[17,22,36] We believe that the carrier mobilities of the single-crystal TPGGs grown on liquid Cu can be further improved by using boron nitride dielectric[37] to reduce the charge trap in the SiO_2 surface or fabricating the suspended devices.

In summary, we controlled the growth of TPGGs and also investigated the effects of the carbon flow rate on the graphene shape change. The as-grown TPGGs were characterized as monolayer and single-crystal features. The whole process from a hexagonal to a twelve-pointed shape was discovered and their relationship was also probed. An edge-diffusion limited growth mechanism was proposed to explain the formation of tips in graphene islands with sizes beyond a critical size of 12.5 μm. High-performance FET devices were successfully achieved based on the as-grown single-crystal grains. It is believed that the TPGGs will provide a profound understanding for the mechanism of graphene growth and find its potential in graphene-based applications.

Experimental Section

50 μm thick Cu foils (99.8% purity) and 100 μm thick W foils (99.95% purity) were employed. 2–4 pieces of Cu foils were directly placed on

Figure 5. Electrical characterization of the single-layer TPGG. (a) Schematic showing the structure of graphene-based FET device. (b) The transfer curve of the TPGG-based FET under N_2 conditions.

the W foil. Before graphene growth, the 1 inch quartz tube was pumped to ~10 Pa to clean the whole system. Then 200 sccm (standard cubic centimeters per minute) H_2 gas flow was filled into the tube. After that, the quartz tube was heated by furnace (Lindberg/Blue M, TF55035A) to 1120 °C for 40–50 min. Next, annealing treatment was performed in pure H_2 gas for 30 min. In the graphene growth process, the H_2 flow rate was set to the required value, and CH_4 was then introduced into the chamber. Finally, CH_4 was turned off, and the system was rapidly cooled down to room temperature.

The TPGGs were characterized by SEM (Hitachi S-4800, 1 kV), optical microscopy, Raman spectroscopy (Renishaw Invia plus, with laser excitation of 514 nm and spot size of 1–2 μm), and TEM (Tecnai G2 F20 U-TWIN, operated at 200 kV). The STM system was an ultra-high vacuum four probe SPM from UNISOKU. AFM images were obtained with a Vecco Nanoscope in tapping mode, at a scan rate of 1.2 Hz and 512×512 resolutions. The electrical characteristics of the FET devices based on individual TPGG on the 300 nm SiO_2/Si substrates were measured by using a Keithley 4200 semiconductor parameter analyzer at room temperature in N_2. The mobility of charge carriers was calculated from the equation: $\mu_{dev} = \frac{L}{V_D C_{ox} W} \cdot \frac{dI_d}{dV_g}$, where L and W are the device channel length and width, respectively, V_D is the voltage between the source and drain electrodes, and C_{ox} is the gate capacitance per unit area.

Supporting Information

Supporting Information is available from the Wiley Online Library or from the author.

[1] K. S. Novoselov, A. K. Geim, S. V. Morozov, D. Jiang, Y. Zhang, S. V. Dubonos, I. V. Grigorieva, A. S. Firsov, *Science* **2004**, *306*, 666.

[2] Y. N. Meng, Y. Zhao, C. G. Hu, H. H. Cheng, Y. Hu, Z. P. Zhang, G. Q. Shi, *Adv. Mater.* **2013**, *25*, 2326.

[3] S. L. Xue, J. W. Dong, L. J. Pan, X. F. Que, Y. D. Zheng, Y. Shi, X. R. Wang, *Nano Res* **2012**, *5*, 361.

[4] K. S. Kim, Y. Zhao, H. Jang, S. Y. Lee, J. M. Kim, K. S. Kim, J. H. Ahn, P. Kim, J. Y. Choi, B. H. Hong, *Nature* **2009**, *457*, 706.

[5] X. S. Li, W. W. Cai, J. An, S. Kim, J. Nah, D. Yang, R. Piner, A. Velamakanni, I. Jung, E. Tutuc, S. K. Banerjee, L. Colombo, R. S. Ruoff, *Science* **2009**, *324*, 1312.

[6] A. W. Robertson, J. H. Warner, *Nano Lett.* **2011**, *11*, 1182.

[7] B. Wu, D. C. Geng, Y. L. Guo, L. P. Huang, Y. Z. Xue, J. Zheng, J. Y. Chen, G. Yu, Y. Q. Liu, L. Jiang, W. P. Hu, *Adv. Mater.* **2011**, *23*, 3522.

[8] I. Vlassiouk, M. Regmi, P. Fulvio, S. Dai, P. Datskos, G. Eres, S. Smirnov, *ACS Nano* **2011**, *5*, 6069.

[9] Q. K. Yu, L. A. Jaurengui, W. Wu, R. Colby, J. Tian, Z. H. Su, H. Cao, Z. Liu, D. Pandey, D. Wei, T. F. Chung, P. Peng, N. P. Guisinger, E. A. Stach, J. Bao, S. S. Pei, Y. P. Chen, *Nat. Mater.* **2011**, *10*, 443.

[10] X. S. Li, C. W. Magnuson, A. Venugopal, R. M. Tromp, J. B. Hannon, E. M. Vogel, L. Colombo, R. S. Ruoff, *J. Am. Chem. Soc.* **2011**, *133*, 2816.

[11] X. Chen, S. Y. Liu, L. C. Liu, X. Q. Liu, X. M. Liu, L. Wang, *Appl. Phys. Lett.* **2012**, *100*, 163106.

[12] J. W. Liu, J. Wu, C. M. Edwards, C. L. Berrie, D. Moore, Z. J. Chen, V. A. Maroni, M. P. Paranthaman, A. Goyal, *Adv. Funct. Mater.* **2011**, *21*, 3868.

[13] Y. A. Wu, A. W. Robertson, F. Schäffel, S. C. Speller, J. H. Warner, *Chem. Mater.* **2011**, *23*, 4543.

[14] H. Ago, I. Tanaka, C. M. Orofeo, M. Tsuji, K. Ikeda, *Small* **2010**, *6*, 1226.

[15] H. Wang, G. Z. Wang, P. F. Bao, S. L. Yang, W. Zhu, X. Xie, W. J. Zhang, *J. Am. Chem. Soc.* **2012**, *134*, 3627.

[16] J. M. Wofford, S. Nie, K. F. McCarty, N. C. Bartelt, O. D. Dubon, *Nano Lett.* **2010**, *12*, 4890.

[17] B. Wu, D. C. Geng, Z. P. Xu, Y. L. Guo, L. P. Huang, Y. Z. Xue, J. Y. Chen, G. Yu, Y. Q. Liu, *NPG Asia Mater.* **2013**, *5*, e36.

[18] M. Massicotte, V. Yu, E. Whiteway, D. Vatnik, M. Hilke, *Nanotechnology* **2013**, *24*, 325601.

[19] R. M. Jacobberger, M. S. Arnold, *Chem. Mater.* **2013**, *25*, 871.

[20] Y. F. Hao, M. S. Bharathi, L. Wang, Y. Y. Liu, H. Chen, S. Nie, X. H. Wang, H. Chou, C. Tan, B. Fallahazad, H. Ramanarayan, C. W. Magnuson, E. Tutuc, B. I. Yakobson, K. F. McCarty, Y. W. Zhang, P. Kim, J. Hone, L. Colombo, R. S. Ruoff, *Science* **2013**, *342*, 720.

[21] T. Ma, W. C. Ren, X. Y. Zhang, Z. B. Liu, Y. Gao, L. C. Yin, X. L. Ma, F. Ding, H. M. Cheng, *Proc. Natl. Acad. Sci. USA* **2013**, *110*, 20386.

[22] D. C. Geng, B. Wu, Y. L. Guo, L. P. Huang, Y. Z. Xue, J. Y. Chen, G. Yu, L. Jiang, W. P. Hu, Y. Q. Liu, *Proc. Natl. Acad. Sci. USA* **2012**, *109*, 7992.

[23] Y. A. Wu, Y. Fan, S. Speller, G. L. Creeth, J. T. Sadowski, K. He, A. W. Robertson, C. S. Allen, J. H. Warner, *ACS Nano* **2012**, *6*, 5010.

[24] Y. Wang, Y. Zheng, X. F. Xu, E. Dubuisson, Q. L. Bao, J. Lu, K. P. Loh, *ACS Nano* **2011**, *5*, 9927.

[25] L. B. Gao, W. C. Ren, H. L. Xu, L. Jin, Z. X. Wang, T. Ma, L. P. Ma, Z. Y. Zhang, Q. Fu, L. M. Peng, X. H. Bao, H. M. Cheng, *Nat. Commun.* **2012**, *3*, e699.

[26] D. C. Geng, B. Wu, Y. L. Guo, B. R. Luo, Y. Z. Xue, J. Y. Chen, G. Yu, Y. Q. Liu, *J. Am. Chem. Soc.* **2013**, *135*, 6431.

[27] Z. W. Shi, R. Yang, L. C. Zhang, Y. Wang, D. H. Liu, D. X. Shi, E. G. Wang, G. Y. Zhang, *Adv. Mater.* **2011**, *23*, 3061.

[28] L. C. Zhang, Y. Wang, Z. W. Shi, D. X. Shi, H. J. Gao, E. G. Wang, G. Y. Zhang, *Adv. Mater.* **2010**, *22*, 4014.

[29] B. R. Luo, H. T. Liu, L. L. Jiang, L. Jiang, D. C. Geng, B. Wu, W. P. Hu, Y. Q. Liu, G. Yu, *J. Mater. Chem. C* **2013**, *1*, 2990.

[30] T. Michely, J. Krug, *Islands, Mounds and Atoms: Patterns and Processes in Crystal Growth Far from Equilibrium*, Springer, New York, USA **2004**.

[31] V. I. Artyukhov, Y. Liu, B. I. Yakobson, *Proc. Natl. Acad. Sci. USA* **2012**, *109*, 15136.

[32] A. Pimpinelli, R. Ferrando, *Phys. Rev. B* **1999**, *60*, 17016.

[33] G. S. Bales, D. C. Chrzan, *Phys. Rev. Lett.* **1995**, *74*, 4879.

[34] P. Lauffer, K. V. Emtsev, R. Graupner, T. Seyller, L. Ley, *Phys. Rev. B* **2008**, *77*, 155426.

[35] D. C. Wei, Y. H. Lu, C. Han, T. C. Niu, W. Chen, A. T. Wee, *Angew. Chem. Int. Ed.* **2013**, *52*, 14121.

[36] J. Wang, M. Q. Zeng, L. F. Tan, B. Y. Dai, Y. Deng, M. Rümmeli, H. T. Xu, Z. S. Li, S. Wang, L. M. Peng, J. Eckert, L. Fu, *Sci. Rep.* **2013**, *3*, e2670.

[37] W. Pan, J. L. Xiao, J. W. Zhu, C. X. Yu, G. Zhang, Z. H. Ni, K. Watanabe, T. Taniguchi, Y. Shi, X. R. Wang, *Sci. Rep.* **2012**, *2*, e893.

ADVANCED MATERIALS

Supporting Information

Controlled Growth of Single-Crystal Twelve-Pointed Graphene Grains on Liquid Cu Surface

Dechao Geng, Lan Meng, Bingyan Chen, Enlai Gao, Wei Yan, Hui Yan, Birong Luo, Jie Xu, Huaping Wang, Zupan Mao, Zhiping Xu, Lin He, Zhiyong Zhang, Lianmao Peng, and Gui Yu*

Supporting Information

Controlled Growth of Single-Crystal Twelve-Pointed Graphene Grains on Liquid Cu Surface

Dechao Geng, Lan Meng, Bingyan Chen, Enlai Gao, Wei Yan, Hui Yan, Birong Luo, Jie Xu, Huaping Wang, Zupan Mao, Zhiping Xu, Lin He, Zhiyong Zhang, Lianmao Peng, and Gui Yu*

Contents

S1. Growth conditions of graphene grains and their characterization

S2. Theoretical analysis of the growth mechanism

S1. Growth conditions of graphene grains and their characterization

Table S1. Growth conditions for three kinds graphene grains.

Graphene shape	Growth temperature (^{o}C)	CH_4 flow rate (sccm)	H_2 flow rate (sccm)	Growth Time (min)
hexagonal	1120	1–2	300	10–25
twelve-pointed	1120	3–5	300	3–5
round	1120	6–10	300	1–3

Table S2. Six diagonal distances of 15 TPGG.

Sample	L_{AG} (μm)	L_{BH} (μm)	L_{CI} (μm)	L_{DJ} (μm)	L_{EK} (μm)	L_{FL} (μm)	$L_{Average}$ (μm)	Standard Deviation
1	36.6	35.8	35.8	36.0	36.5	37.0	36.3	0.492
2	41.0	40.9	40.1	40.1	40.4	40.4	40.5	0.387
3	42.7	42.9	43.1	42.9	43.2	43.7	43.1	0.349
4	42.3	42.4	42.0	42.3	42.4	42.2	42.3	0.151
5	37.3	38.2	37.2	38.4	37.7	38.3	37.9	0.524
6	36.0	36.3	36.9	36.7	36.4	36.5	36.5	0.314
7	42.6	42.9	42.4	42.5	42.3	43.4	42.7	0.407

| 8 | 35.6 | 35.1 | 35.1 | 34.8 | 34.9 | 34.8 | 35.1 | 0.302 |
9	34.6	34.1	34.4	34.6	34.7	34.9	34.6	0.274
10	31.9	31.3	31.8	31.2	31.1	31.5	31.5	0.327
11	28.3	28.7	28.8	28.6	28.3	28.9	28.6	0.253
12	31.3	32.1	31.7	32.2	31.9	32.0	31.9	0.327
13	27.4	27.2	27.6	26.9	27.1	27.1	27.2	0.248
14	43.6	44.2	43.3	43.2	42.8	43.3	43.4	0.469
15	23.7	24.0	23.4	24.5	23.9	24.0	24.0	0.366
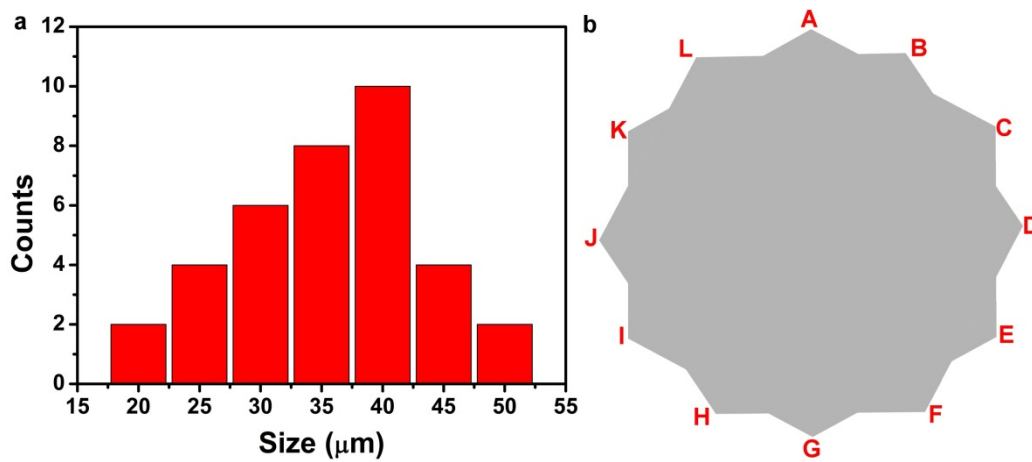
Figure S1. (a) Size statistics of 15 TPGGs. (b) Six diagonal distances of single grains, identified as AG, BH, CI, DJ, EK and FL, respectively. The detailed statistics of diagonal values are listed in Table S2.
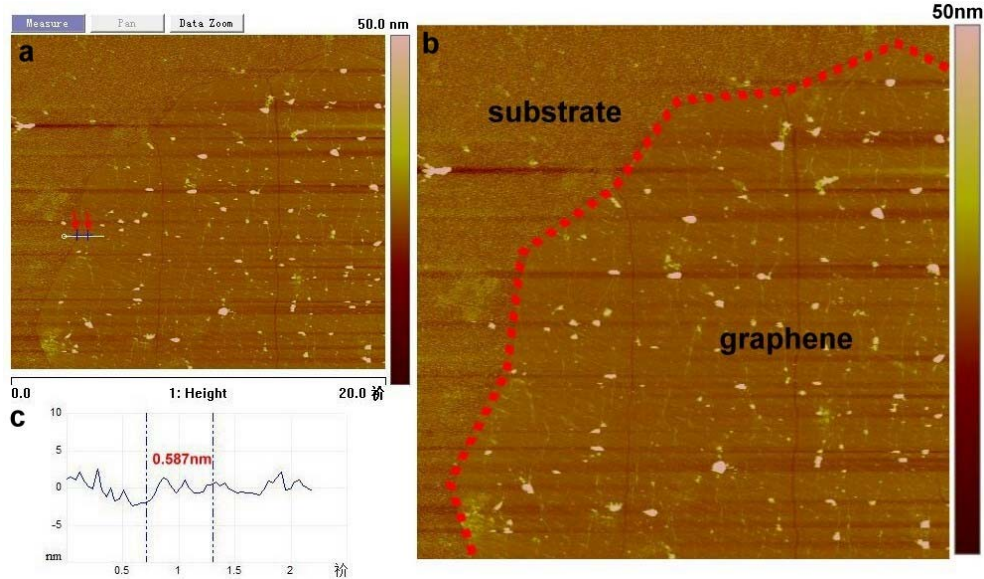
Figure S2. AFM measurements of the TPGG transferred onto SiO$_2$/Si substrate. (a, b) Surface morphology of single grain. (c) Height profiles across patterned graphene edges.
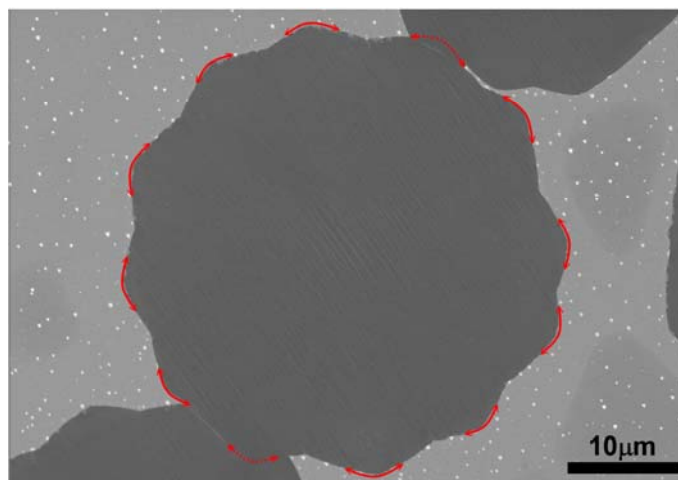

Figure S3. SEM image of blunt TPGG.
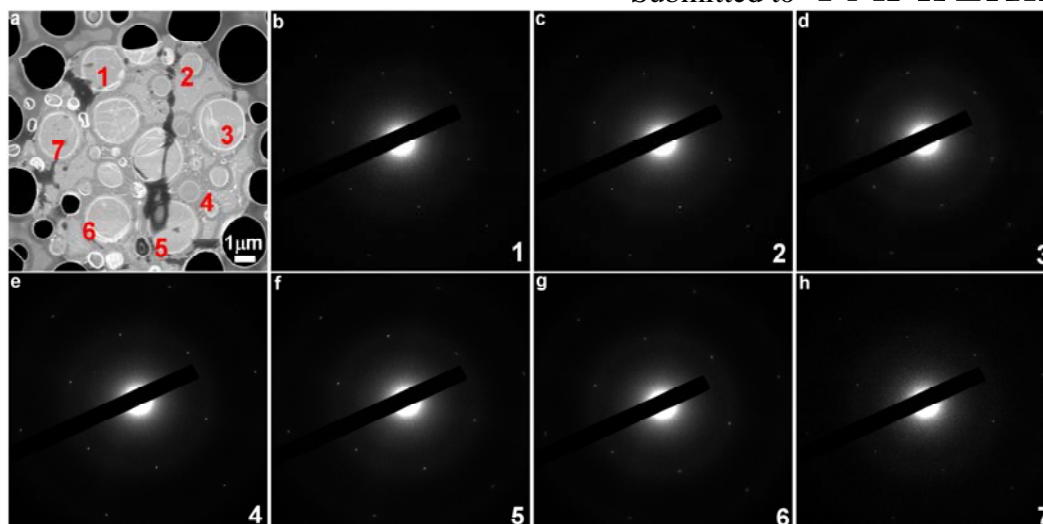
Figure S4. Electron diffraction of the blunt TPGGs. (a) SEM image of the blunt TPGGs transferred onto a copper grid. (b-h) SEAD data for small regions of single graphene grain indicated 1 to 7.
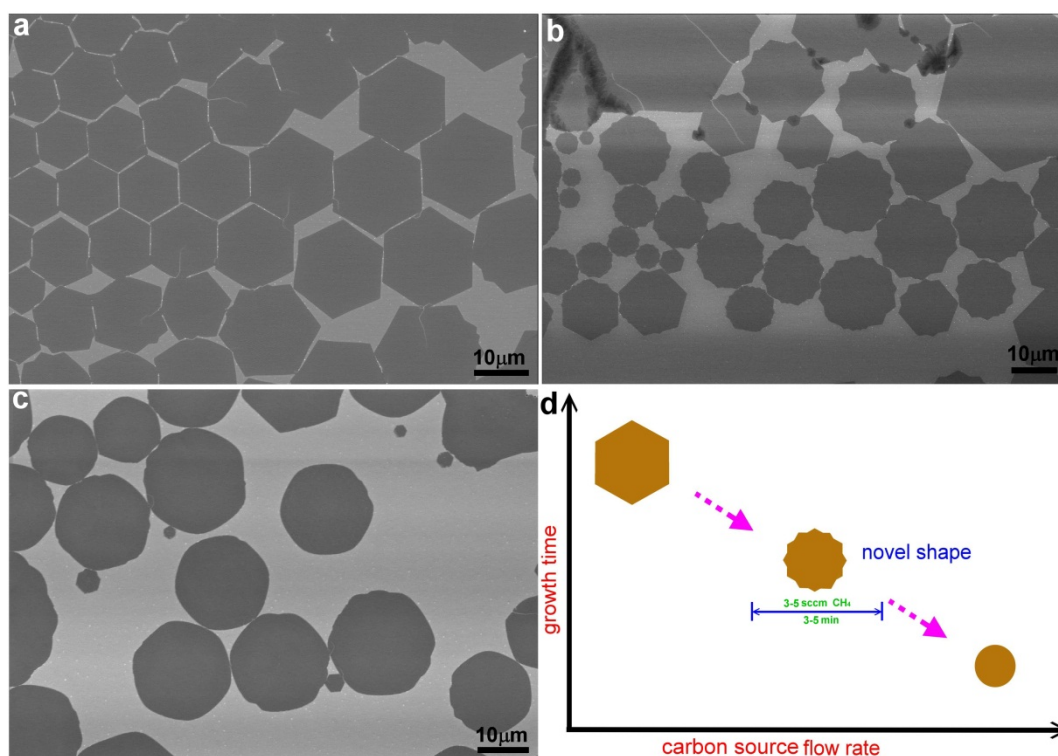

Figure S5. Shape change of graphene grains as increase of carbon flow rate. (a-c) SEM images of the hexagonal, twelve-pointed, and round graphene grains fabricated under the growth conditions of Table S1. (d) Model of the transforming process of the three shape graphene grains.
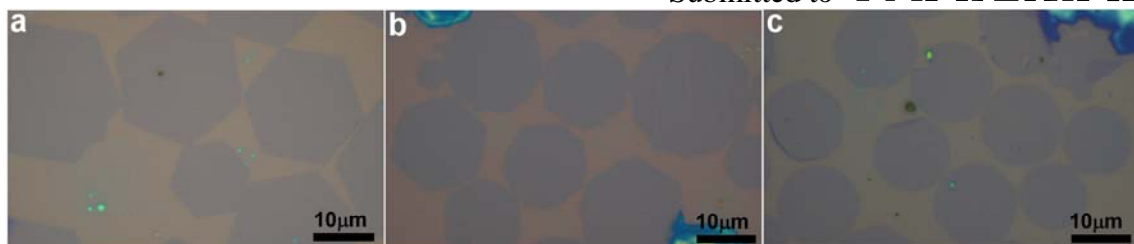
Figure S6. The optical images of large-area and clean (a) hexagonal, (b) twelve-pointed, and (c) round graphene grains transferred onto 300 nm Si/SiO$_2$ substrates.
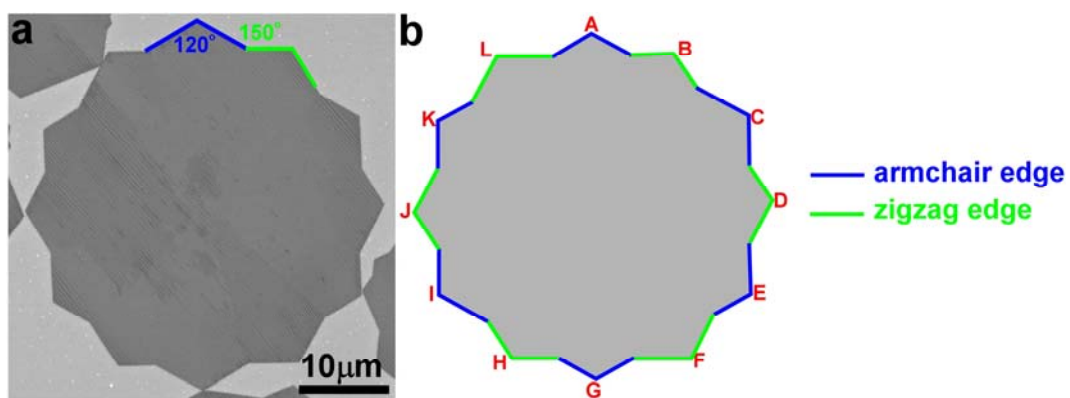
**Figure S7.** The edge characteristics of twelve-pointed graphene grain.
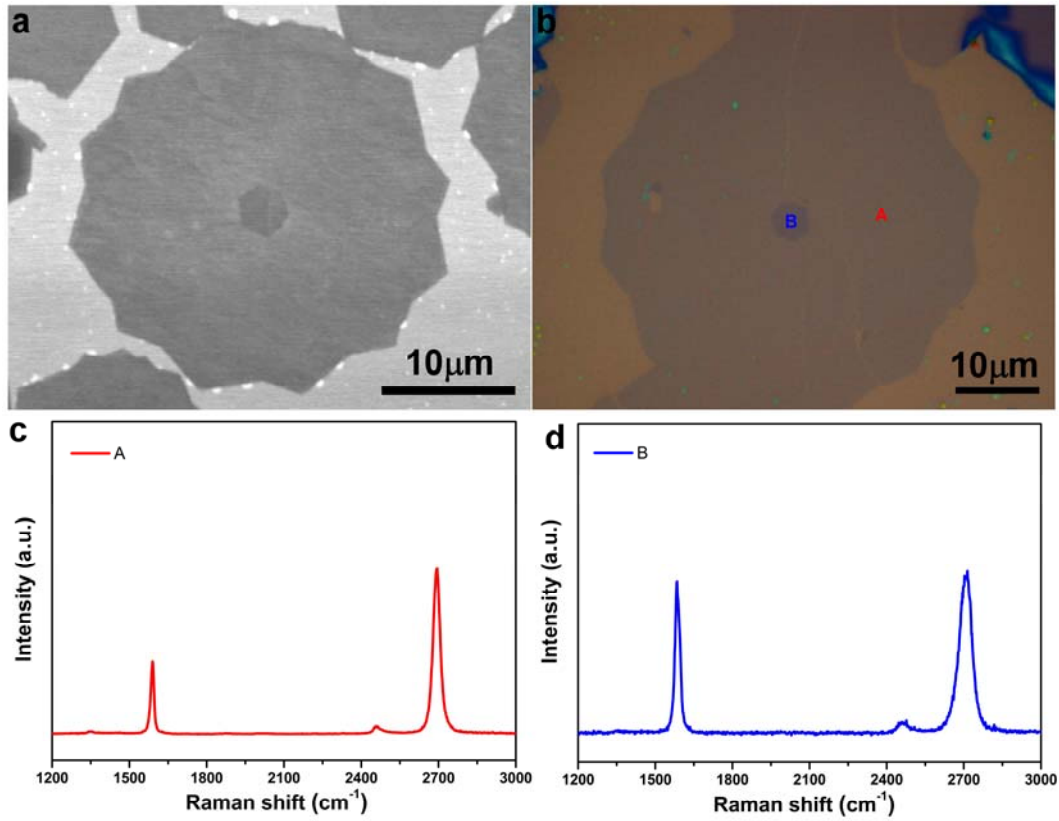
Figure S8. Characterizations of the as-grown bilayer TPGG. (a) SEM image of the bilayer TPGG prepared on liquid Cu surface. (b) Optical image of the bilayer TPGG transferred onto Si/SiO$_2$ substrate. (c, d) Raman spectrum of the parts labeled as A and B in (b).
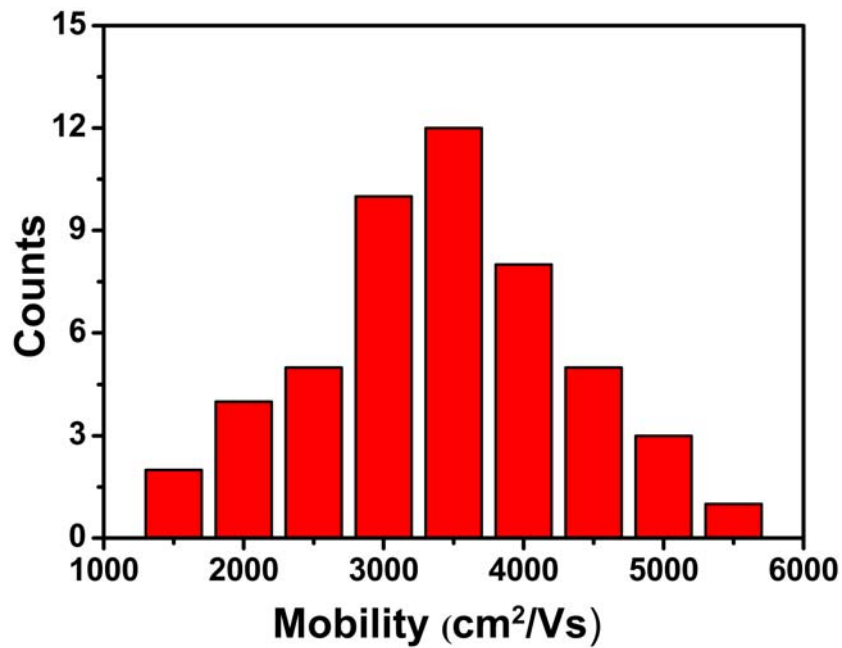
Figure S9. Statistical histogram of hole mobility distribution for the TPGGs.
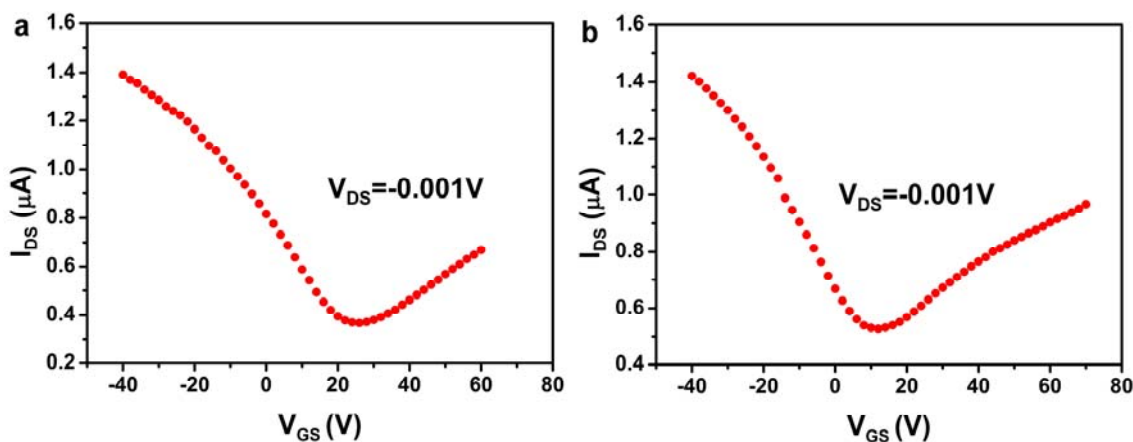
Figure S10. The transfer curves of the FET devices based on (a) hexagonal and (b) twelve-pointed graphene grains under the same device fabrication method and configuration.

S2. Theoretical analysis of the growth mechanism
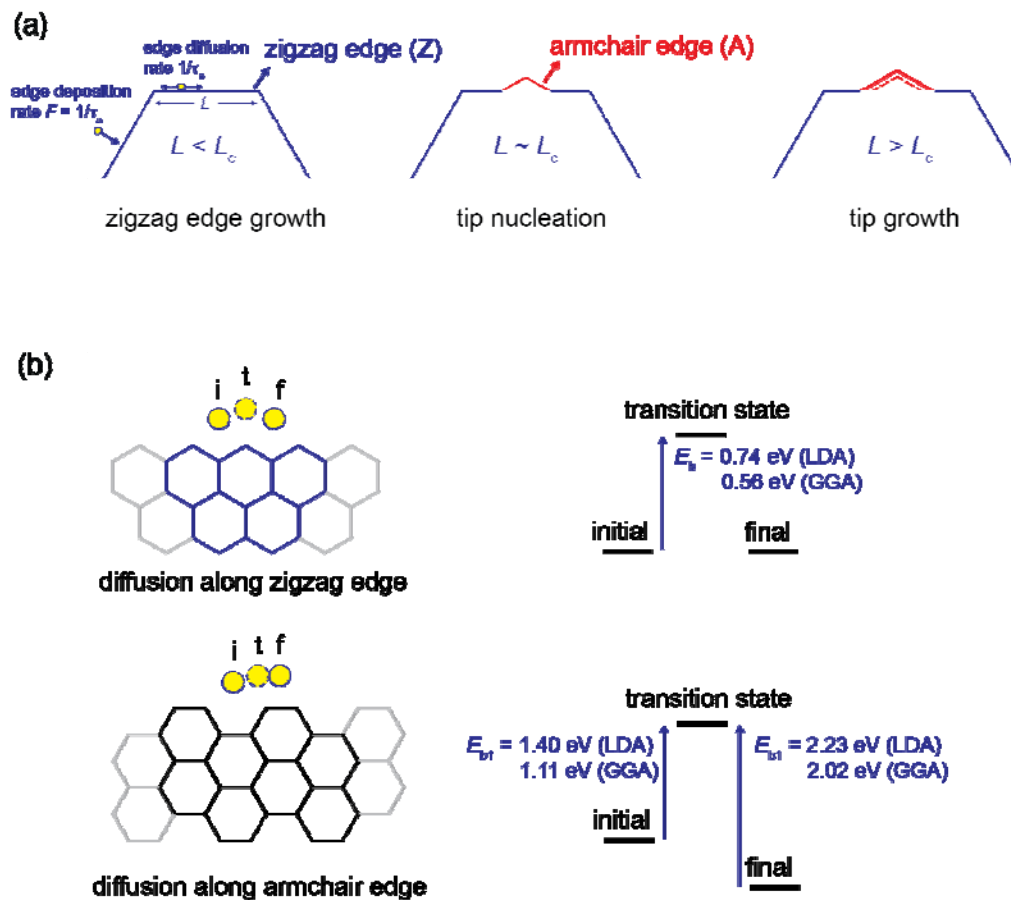
1. The edge-diffusion limited growth mechanism

The edge-diffusion limited mechanism introduced in the text is illustrated here in **Figure S11a**. Armchair triangular islands with higher growth rate nucleate once the edge length L exceeds a critical length L_c defined by the diffusion coefficient along graphene edges D_e and carbon deposition rate $1/\tau_a$. The preferred edge diffusion from zigzag edges to armchair edges with lower edge energy after the tips nucleate further advance the growth of armchair edges.[1]

2. First-principles calculations of the edge diffusion paths

To explore the diffusion paths and diffusion barriers of carbon atoms along the graphene edges, we perform density functional theory (DFT) based first-principles calculations. The graphene edges are modeled by four super-cells of graphene nanoribbons. The plane-wave code Quantum-Espresso is used here with a kinetic energy cutoff of 60 Ry.[2] We use ultra-soft pseudopotentials[3] for the core-valence electron interaction, and implement both the Perdew-Zunger parametrization of local density approximation (LDA)[4] and the Perdew-Burke-Ernzerhof (PBE) parametrization of generalized gradient approximation (GGA)[5] for the exchange-correlation functional. These settings are verified to achieve a total energy convergence for the systems under exploration below 1 meV/atom. 12 Monkhorst-Pack k-points are used in periodic directions and vacuum layers of 2 nm are used in non-periodic

7

ones. The atomic structures are relaxed before calculating diffusive reaction barriers E_b using the nudged elastic band (NEB) technique.[6]

The calculated energy barriers are summarized in **Figure S11b**. Although LDA tends to overbind atoms in DFT calculations and yields higher barrier heights, the results are in general consistent with those calculated from GGA. With GGA, the diffusion barriers along the zigzag edge is 0.56 eV, while for the armchair edge E_b = 2.02 eV. These results clearly indicate that at the growth condition with temperature ~ 1400 K, edge diffusion is activated and plays a dominant role in competing with edge deposition of carbon atoms as discussion previously. Quantitative predictions, however, require further knowledge about the edge deposition rate F, and possible changes in the diffusive process with the presence of copper substrate should also be considered.

(a)

edge diffusion rate $1/\tau_a$ zigzag edge (Z)   armchair edge (A)

edge deposition rate $F = 1/\tau_a$

$L < L_c$ $L \sim L_c$ $L > L_c$

zigzag edge growth   tip nucleation   tip growth

(b)

i t f

diffusion along zigzag edge

transition state

E_a = 0.74 eV (LDA)
0.56 eV (GGA)

initial   final

i t f

diffusion along armchair edge

transition state

E_{b1} = 1.40 eV (LDA)
1.11 eV (GGA)

E_{b1} = 2.23 eV (LDA)
2.02 eV (GGA)

initial

final

Figure S11. (a) The edge-diffusion limited graphene grain growth mechanism, where armchair triangular islands nucleate when the edge length exceeds a critical length L_c defined by the diffusion coefficient along graphene edges D_e and carbon deposition rate $1/\tau_a$. (b) Diffusion barriers for carbon atoms along zigzag and armchair edges. Values are obtained based on both LDA and GGA based exchange-correlation functionals.

References

[1] T. Michely, J. Krug, *Islands, Mounds and Atoms: Patterns and Processes in Crystal Growth Far from Equilibrium*, Springer, New York, USA **2004**.

[2] P. Giannozzi, S. Baroni, N. Bonini, M. Calandra, R. Car, C. Carlo, C. Davide, L. C. Guido, C. Matteo, D. Ismaila, C. Andrea Dal, G. Stefano de, F. Stefano, F. Guido, G. Ralph, G. Uwe, G. Christos, K. Anton, L. Michele, M. S. Layla, M. Nicola, M. Francesco, M. Riccardo, P. Stefano, P. Alfredo, P. Lorenzo, S. Carlo, S. Sandro, S. Gabriele, P. S. Ari, A. Smogunov, P. Umari, R. M. Wentzcovitch, *J. Phys.: Condens. Matter* **2009**, *21*, 395502.

[3] D. Vanderbilt, *Physical Review B* **1990**, *41*, 7892.

[4] J. P. Perdew, A. Zunger, *Physical Review B* **1981**, *23*, 5048.

[5] J. P. Perdew, K. Burke, M. Ernzerhof, *Phys. Rev. Lett.* **1996**, *77*, 3865.

[6] G. Henkelman, B. P. Uberuaga, H. Jónsson, *J. Chem. Phys.* **2000**, *113*, 9901.